Permanent Magnet Synchronous Motor Control Algorithm Based on Stability Margin and Lyapunov Stability Analysis

Hongyu Jie[†], Hongbing Xu[*], Yanbing Zheng[*], Xiaoshuai Xin[*], and Gang Zheng[*]

[†,*]School of Automation Engineering, University of Electronic Science and Technology of China, Chengdu, China

Abstract

The permanent magnet synchronous motor (PMSM) is widely used in various fields and the proportional-integral (PI) controller is popular in PMSM control systems. However, the motor parameters are usually unknown, which can lead to a complicated PI controller design and poor performance. In order to design a PI controller with good performance when the motor parameters are unknown, a control algorithm based on stability margin is proposed in this paper. First of all, based on the mathematical model of the PMSM and the least squares (LS) method, motor parameters are estimated offline. Then based on the estimation values of the motor parameters, natural angular frequency and phase margin, a PI controller is designed. Performance indices including the natural angular frequency and the phase margin are used directly to design the PI controller in this paper. Scalar functions of the d-loop and the q-loop are selected. It can be seen that the designed controller parameters satisfy Lyapunov large scale asymptotic stability theory if the natural angular frequencies of the d-loop and the q-loop are large than 0. Experimental results show that the parameter estimation method has good accuracy and the designed PI controller proposed in this paper has good static and dynamic performances.

Key words: Least squares, Natural angular frequency, Parameter estimation, Permanent magnet synchronous motor, Phase margin, Proportional-integral controller, Stability margin

I. INTRODUCTION

Due to its advantages, including simple structure, small volume, high power density, high efficiency, high reliability, and rapid response, the PMSM has been widely used in various fields such as electric vehicles, industrial control, consumer electronics, etc. [1]. Moreover, for PMSM control systems, there is no doubt that the classical PI control algorithm is still popular due to its simple structure and high reliability [2]. In addition, the vector control (VC) strategy is still important since it possesses the characteristics of accurate torque control, wide speed range and rapid response [3]. However, the motor parameters are usually unknown, which can lead to a complicated PI controller design and poor performance. Thus, a method to design a PI controller with

good performance when the motor parameters are unknown has become a key issue in PMSM control.

Some work has already been done to design the PI controllers of the PMSM. Manipulation tuning is a frequently-used method to design PI control parameters. However, a lot of time and effort are needed to regulate the PI control parameters to obtain good performance [4]. In addition to the manipulation tuning method, the BODE diagram method [5], relay feedback method [6] and Ziegler-Nichols engineering method [7], [8], have also been used to design PI control parameters. However, a lot of experiments and experience are needed in these methods. Meanwhile, an unstable control effect may occur during experiments. In addition, some intelligent algorithms such as the neural networks method [9], [10], genetic algorithm [11], [12], fuzzy logic method [13], [14], artificial bee colony algorithm [15], co-efficient diagram method [16] and improved just-in-time learning technique [17], [18] have been used to implement the design of PI control parameters. The adaptability and robustness of systems have been improved through these methods. However, these

methods are complicated and have high hardware performance requirements.

Some work has also been done to estimate the parameters of the PMSM. In [19], [20], the model reference adaptive scheme (MRAS) is presented to estimate PMSM's parameters. However, extensive experience and multiple experiments are required in this approach. In [21], [22], the extended Kalman filter (EKF) method is presented to estimate the PMSM's parameters. The EKF method can avoid the problem of noise sensitivity and simultaneously estimate the states and parameters. However, it contains some matrix inversion operations, which require a lot of calculations. In [23], [24], the neural network method is applied to estimate the parameters of PMSM. However, this method cannot guarantee its own stability and the convergence of the estimation values. In [25], Popov's stability criterion is applied to estimate PMSM's parameters and the estimation values are accurate. In [26], an evolution algorithm based on immune particle swarm optimization (PSO) is proposed to estimate the parameters of PMSM. However, this method is complicated in design and implementation. In [27]-[29], the least squares (LS) method is applied to estimated PMSM's parameters. This method is easy to implement in terms of its program and it is accurate, which makes it useful for the parameter estimation in this paper.

In order to design a PI controller with good performance when the motor parameters are unknown, a control algorithm based on stability margin is proposed in this paper. First of all, based on the mathematical model of the PMSM and the LS method, motor parameters are estimated offline. Then based on the estimated values of the motor parameters, natural angular frequency and phase margin, a PI controller is designed. Performance indices including the natural angular frequency and phase margin are directly used to design the PI controller in this paper.

This paper is organized as follows. The VC mathematical model of the PMSM is presented in Section II. In addition, the control laws of the d-loop and the q-loop of the PMSM VC system based on the stability margin are obtained in this section. Parameter estimation of the PMSM is presented in Section III. At the same time, according to the estimation values, the final control laws of the d-loop and the q-loop of the PMSM VC system are obtained in this section. The Lyapunov stability analysis is presented in Section IV. Experimental results are shown in Section V. Finally, some conclusions are given in Section VI.

II. VC MATHEMATICAL MODEL OF THE PMSM

The armature circuit of the three-phase AC PMSM is usually equivalent to a first order inertial element with a stator resistance (R_s) and a stator inductance. Thus, the transfer functions of the d-loop and the q-loop of the PMSM

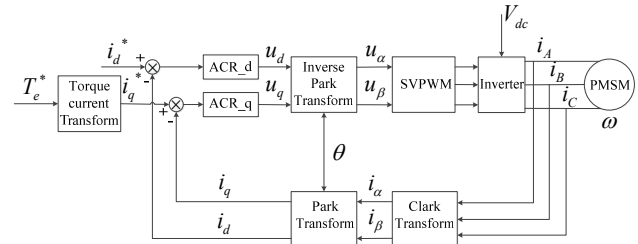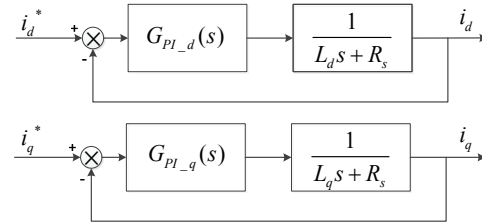Fig. 1. Block diagram of the PMSM VC system.

Fig. 2. Structure diagram of the PMSM VC system.

with respect to d-q coordinate can be described as is shown in equations (1) and (2).

$$G_d(s) = \frac{i_d(s)}{u_d(s)} = \frac{1}{L_d s + R_s} \qquad (1)$$

$$G_q(s) = \frac{i_q(s)}{u_q(s)} = \frac{1}{L_q s + R_s} \qquad (2)$$

where u_d and u_q are the voltages of the d-loop and the q-loop; i_d and i_q are the currents of the d-loop and the q-loop; and L_d and L_q are the inductances of the d-loop and the q-loop, respectively.

Generally, a PI controller is adopted to regulate the current of the d-loop and the q-loop. The block diagram of the PMSM VC system is presented in Fig. 1.

In Fig. 1, T_e^* is the expected electromagnetic torque; i_d^* and i_q^* are the expected currents of the d-loop of the q-loop; u_α and u_β are the voltages of the α-axis and the β-axis; i_α and i_β are the currents of the α-axis and the β-axis; V_{dc} is the voltage of the DC bus; i_A, i_B and i_C are the currents of A-axis, B-axis and C-axis; θ is the electrical angle; ω is the speed; ACR_d is the d-loop PI controller; and ACR_q is the q-loop PI controller.

In Fig. 1, the delay generated by the inverter (the control period of inverter) is usually in the microsecond range. However, the time constant of the PMSM is in the millisecond range and is much larger than the delay generated by the inverter. According to the control theory, the link with this small time constant can be ignored when the mathematical model is established. Thus, the delay generated by the inverter is ignored in this paper. Then, in terms of the VC principle, the structure diagram of the PMSM VC system is presented in Fig. 2.

The transfer functions of the d-loop PI controller and the q-loop PI controller are shown in equation (3) and equation (4), respectively.

$$G_{PI\_d}(s) = \frac{K_{p\_d}s + K_{i\_d}}{s} \qquad (3)$$

$$G_{PI\_q}(s) = \frac{K_{p\_q}s + K_{i\_q}}{s} \qquad (4)$$

where K_{p_d} is the proportion factor of the d-loop PI controller; K_{i_d} is the integral factor of the d-loop PI controller; K_{p_q} is the proportion factor of the q-loop PI controller; K_{i_q} is the integral factor of the q-loop PI controller.

Based on equations (1), (2), (3) and (4), the closed-loop transfer functions of the d-loop and the q-loop are obtained as is shown in equations (5) and (6), respectively.

$$\Phi_d(s) = \frac{i_d(s)}{i_d^*(s)} = \frac{K_{p\_d}s + K_{i\_d}}{L_d s^2 + R_s s + K_{p\_d}s + K_{i\_d}} \qquad (5)$$

$$\Phi_q(s) = \frac{i_q(s)}{i_q^*(s)} = \frac{K_{p\_q}s + K_{i\_q}}{L_q s^2 + R_s s + K_{p\_q}s + K_{i\_q}} \qquad (6)$$

Obviously, according to equations (5) and (6), the d-loop and the q-loop are changed into a second order element. In addition, the closed-loop characteristic formula of a typical second order system is presented as is shown in equation (7).

$$s^2 + 2\zeta\omega_n s + \omega_n^2 = 0 \qquad (7)$$

where ζ is damping coefficient; and ω_n is natural angular frequency.

According to the coefficient comparison method, the coefficient of the term of s between equation (5) and equation (7) should be equal, and the constant term should be equal, which is the same as equation (6) and equation (7). This can be explained in detail, as is shown in equations (8) through (11).

$$2\zeta_d\omega_{nd} = \frac{R_s + K_{p\_d}}{L_d} \qquad (8)$$

$$\omega_{nd}^2 = \frac{K_{i\_d}}{L_d} \qquad (9)$$

$$2\zeta_q\omega_{nq} = \frac{R_s + K_{p\_q}}{L_q} \qquad (10)$$

$$\omega_{nq}^2 = \frac{K_{i\_q}}{L_q} \qquad (11)$$

where ζ_d and ζ_q are the damping coefficients of the d-loop and the d-loop; and ω_{nd} and ω_{nq} are the natural angular frequencies of the d-loop and the q-loop, respectively.

In this paper, system performance indices including the natural angular frequency and phase margin of the d-loop, and the natural angular frequency and phase margin of the q-loop are selected as is shown in equations (12) through (15).

$$\gamma_d = \frac{\pi}{2} - \arctan\frac{\omega_{cd}}{2\zeta_d\omega_{nd}} \qquad (12)$$

$$\gamma_q = \frac{\pi}{2} - \arctan\frac{\omega_{cq}}{2\zeta_q\omega_{nq}} \qquad (13)$$

$$\zeta_d = (\frac{1}{(4*(\cot\gamma_d)^2 + 2)^2 - 4})^{\frac{1}{4}} \qquad (14)$$

$$\zeta_q = (\frac{1}{(4*(\cot\gamma_q)^2 + 2)^2 - 4})^{\frac{1}{4}} \qquad (15)$$

where ω_{cd} and ω_{cq} are the cut-off frequencies of the d-loop and the q-loop; and γ_d and γ_q are the phase margins of the d-loop and the q-loop, respectively.

The calculation equations of ω_{cd} and ω_{cq} are obtained as is shown in equations (16) and (17), respectively.

$$\omega_{cd} = \omega_{nd}(\sqrt{4\zeta_d^4 + 1} - 2\zeta_d^2)^{\frac{1}{2}} \qquad (16)$$

$$\omega_{cq} = \omega_{nq}(\sqrt{4\zeta_q^4 + 1} - 2\zeta_q^2)^{\frac{1}{2}} \qquad (17)$$

According to equations (8) through (17), the calculation equations of the PI controller parameters of the d-loop and the q-loop can be obtained as is shown in equations (18) through (21).

$$K_{p\_d} = f(\omega_{nd}, \gamma_d, L_d)$$
$$= 2\omega_{nd}L_d(\frac{1}{(4(\cot\gamma_d)^2 + 2)^2 - 4})^{\frac{1}{4}} - R_s \qquad (18)$$

$$K_{i\_d} = f(\omega_{nd}, L_d) = L_d\omega_{nd}^2 \qquad (19)$$

$$K_{p\_q} = f(\omega_{nq}, \gamma_q, L_q)$$
$$= 2\omega_{nq}L_q(\frac{1}{(4(\cot\gamma_q)^2 + 2)^2 - 4})^{\frac{1}{4}} - R_s \qquad (20)$$

$$K_{i\_q} = f(\omega_{nq}, L_q) = L_q\omega_{nq}^2 \qquad (21)$$

Therefore, the control laws of the d-loop and the q-loop are shown in equations (22) and (23), respectively.

$$u_d = K_{p\_d}\Delta e_d + K_{i\_d}\int_0^t \Delta e_d dt$$
$$= (2\omega_{nd}L_d(\frac{1}{(4(\cot\gamma_d)^2 + 2)^2 - 4})^{\frac{1}{4}} - R_s)\Delta e_d \qquad (22)$$
$$+ L_d\omega_{nd}^2\int_0^t \Delta e_d dt$$

$$u_q = K_{p\_q}\Delta e_q + K_{i\_q}\int_0^t \Delta e_q dt$$
$$= (2\omega_{nq}L_q(\frac{1}{(4(\cot\gamma_q)^2 + 2)^2 - 4})^{\frac{1}{4}} - R_s)\Delta e_q \qquad (23)$$
$$+ L_q\omega_{nq}^2\int_0^t \Delta e_q dt$$

where Δe_d is the current deviation of the d-loop; and Δe_q is the current deviation of the q-loop.

III. PARAMETER ESTIMATION OF THE PMSM

It is assumed that harmonics, iron consumption, hysteresis loss and eddy current loss are not taken into account.

Thus, the steady-state mathematical model of the PMSM with respect to the d-q coordinate can be described as is

shown in equation (24).

$$\begin{cases} u_q = R_s i_q + \omega_e L_d i_d + \omega_e \psi_f \\ u_d = R_s i_d - \omega_e L_q i_q \end{cases} \tag{24}$$

where ω_e is the electrical angular velocity; and ψ_f is the magnet flux linkage.

From equation (24), the calculation equations of L_q and L_d can be obtained as is shown in equations (25) and (26), respectively.

$$L_q = \frac{-u_d + R_s i_d}{\omega_e i_q} \tag{25}$$

$$L_d = \frac{u_q - \omega_e \psi_f - R_s i_q}{\omega_e i_d} \tag{26}$$

Generally, a digital signal processor is applied to implement PMSM control. From equations (25) and (26), the calculation equations of L_q and L_d can be expressed as is shown in equations (27) and (28), respectively.

$$L_q(k) = \frac{-u_d(k) + R_s i_d(k)}{\omega_e(k) i_q(k)} \tag{27}$$

$$L_d(k) = \frac{u_q(k) - \omega_e(k)\psi_f - R_s i_q(k)}{\omega_e(k) i_d(k)} \tag{28}$$

where $L_q(k)$ and $L_d(k)$ are the estimation values through the k-th samples; $u_q(k)$, $u_d(k)$, $i_q(k)$, $i_d(k)$ and $\omega_e(k)$ are the k-th samples of u_q, u_d, i_q, i_d and ω_e, respectively.

However, some influences such as sampling error can lead to a big error between the estimation value of L_q and the real value of L_q, which is the same as L_d. As a result, the LS method is applied in this paper to make the estimation values more accurate.

Denote:

$$J_d = \sum_{i=1}^{k} \varepsilon_d(i)^2 \tag{29}$$

$$J_q = \sum_{i=1}^{k} \varepsilon_q(i)^2 \tag{30}$$

where $\varepsilon_d(k)$ is defined as $\varepsilon_d(k)=L_d(k)-L_d$; and $\varepsilon_q(k)$ is defined as $\varepsilon_q(k)=L_q(k)-L_q$.

Since the theory of LS is to find a value of $\hat{L}_d$ to minimize J_d and to find a value of $\hat{L}_q$ to minimize J_q, the partial derivative of J_d with respect to L_d and the partial derivative of J_q with respect to L_q could be obtained. Furthermore, the partial derivatives of J_d and J_q should be set to 0. Thus, the minimum J_d and J_q could be obtained when $L_d = \hat{L}_d$ and $L_q = \hat{L}_q$, as is shown in equations (31) and (32), respectively.

$$\frac{\partial J_d}{\partial L_d}\Big|_{L_d = \hat{L}_d} = -2\sum_{i=1}^{k} L_d(i) + 2k\hat{L}_d = 0 \tag{31}$$

$$\frac{\partial J_q}{\partial L_q}\Big|_{L_q = \hat{L}_q} = -2\sum_{i=1}^{k} L_q(i) + 2k\hat{L}_q = 0 \tag{32}$$

In conclusion, $\hat{L}_d$ and $\hat{L}_q$ can be expressed as is shown in equations (33) and (34), respectively.

$$\hat{L}_d = \frac{\sum_{i=1}^{k} L_d(i)}{k} \tag{33}$$

$$\hat{L}_q = \frac{\sum_{i=1}^{k} L_q(i)}{k} \tag{34}$$

According to equations (18) through (21) and equations (33) through (34), the calculation equations of the PI controller parameters of the d-loop and the q-loop can be obtained as is shown in equations (35) through (38).

$$\begin{aligned} K_{p\_d} &= f(\omega_{nd}, \gamma_d, \hat{L}_d) \\ &= 2\omega_{nd} \frac{\sum_{i=1}^{k} L_d(i)}{k} \left(\frac{1}{(4(\cot\gamma_d)^2 + 2)^2 - 4}\right)^{\frac{1}{4}} - R_s \end{aligned} \tag{35}$$

$$K_{i\_d} = f(\omega_{nd}, \hat{L}_d) = \frac{\sum_{i=1}^{k} L_d(i)}{k} \omega_{nd}^2 \tag{36}$$

$$\begin{aligned} K_{p\_q} &= f(\omega_{nq}, \gamma_q, \hat{L}_q) \\ &= 2\omega_{nq} \frac{\sum_{i=1}^{k} L_q(i)}{k} \left(\frac{1}{(4(\cot\gamma_q)^2 + 2)^2 - 4}\right)^{\frac{1}{4}} - R_s \end{aligned} \tag{37}$$

$$K_{i\_q} = f(\omega_{nq}, \hat{L}_q) = \frac{\sum_{i=1}^{k} L_q(i)}{k} \omega_{nq}^2 \tag{38}$$

Finally, the control laws of the d-loop and the q-loop of the PMSM VC system are shown in equations (39) and (40), respectively.

$$\begin{aligned} u_d &= K_{p\_d}\Delta e_d + K_{i\_d}\int_0^t \Delta e_d dt \\ &= (2\omega_{nd} \frac{\sum_{i=1}^{k} L_d(i)}{k} \left(\frac{1}{(4(\cot\gamma_d)^2 + 2)^2 - 4}\right)^{\frac{1}{4}} - R_s)\Delta e_d \\ &+ \frac{\sum_{i=1}^{k} L_d(i)}{k} \omega_{nd}^2 \int_0^t \Delta e_d dt \end{aligned} \tag{39}$$

$$\begin{aligned} u_q &= K_{p\_q}\Delta e_q + K_{i\_q}\int_0^t \Delta e_q dt \\ &= (2\omega_{nq} \frac{\sum_{i=1}^{k} L_q(i)}{k} \left(\frac{1}{(4(\cot\gamma_q)^2 + 2)^2 - 4}\right)^{\frac{1}{4}} - R_s)\Delta e_q \\ &+ \frac{\sum_{i=1}^{k} L_q(i)}{k} \omega_{nq}^2 \int_0^t \Delta e_q dt \end{aligned} \tag{40}$$

IV. ANALYSIS OF STABILITY

Some preconditions are shown in equation (41) before the stability analysis.

$$\begin{cases} L_d > 0 \\ L_q > 0 \\ \omega_{nd} > 0 \cap 0 < \omega^2_{nd} < \infty \\ \omega_{nq} > 0 \cap 0 < \omega^2_{nq} < \infty \\ 0 < \gamma_d < \pi/2 \\ 0 < \gamma_q < \pi/2 \end{cases} \tag{41}$$

The stability in this paper is divided into the stability of the d-loop and the stability of the q-loop, and they both need to be proven. The analyses of the stability between the d-loop and the q-loop are similar. The stability of the d-loop is proven below.

The closed-loop transfer function of the d-loop can be expressed as is shown in equation (42).

$$\Phi_d(s) = \frac{i_d(s)}{i_d^*(s)} = \frac{Y_d(s)}{R_d(s)} = \frac{\dfrac{K_{p\_d}}{L_d} s + \dfrac{K_{i\_d}}{L_d}}{s^2 + \dfrac{R_s + K_{p\_d}}{L_d} s + \dfrac{K_{i\_d}}{L_d}} \tag{42}$$

The state vector x_d is defined as is shown in equation (43), and the conditions which need to be satisfied by the state variables are shown in equation (44). X_d is the state space of the d-loop.

$$x_d = [x_{d1}, x_{d2}]^T \in X_d \tag{43}$$

$$\begin{cases} x_{d1} = L^{-1} \left[\dfrac{1}{s^2 + \dfrac{R_s + K_{p\_d}}{L_d} s + \dfrac{K_{i\_d}}{L_d}} R_d(s) \right] \\ x_{d2} = \dot{x}_{d1} \end{cases} \tag{44}$$

Based on equations (42) and (44), $\dot{x}_{d2}$ and y_d are obtained as is shown in equations (45) and (46), respectively.

$$\dot{x}_{d2} = -\frac{K_{i\_d}}{L_d} x_{d1} - \frac{R_s + K_{p\_d}}{L_d} x_{d2} + r_d \tag{45}$$

$$y_d = \frac{K_{i\_d}}{L_d} x_{d1} + \frac{K_{p\_d}}{L_d} x_{d2} \tag{46}$$

where r_d is the inverse Laplace transformation of $R_d(s)$; and y_d is the inverse Laplace transformation of $Y_d(s)$.

According to equations (44) through (46), the state equation of the d-loop, the homogeneous state equation of the d-loop and the output equation of the d-loop can be obtained as is shown in equations (47), (48) and (49), respectively.

$$\begin{bmatrix} \dot{x}_{d1} \\ \dot{x}_{d2} \end{bmatrix} = \begin{bmatrix} 0 & 1 \\ -\dfrac{k_{i\_d}}{L_d} & -\dfrac{k_{p\_d} + R_s}{L_d} \end{bmatrix} \begin{bmatrix} x_{d1} \\ x_{d2} \end{bmatrix} + \begin{bmatrix} 0 \\ 1 \end{bmatrix} r_d \tag{47}$$

$$\begin{bmatrix} \dot{x}_{d1} \\ \dot{x}_{d2} \end{bmatrix} = \begin{bmatrix} 0 & 1 \\ -\dfrac{k_{i\_d}}{L_d} & -\dfrac{k_{p\_d} + R_s}{L_d} \end{bmatrix} \begin{bmatrix} x_{d1} \\ x_{d2} \end{bmatrix} \tag{48}$$

$$y_d = \begin{bmatrix} \dfrac{k_{i\_d}}{L_d} & \dfrac{k_{p\_d}}{L_d} \end{bmatrix} \begin{bmatrix} x_{d1} \\ x_{d2} \end{bmatrix} \tag{49}$$

Equilibrium states can be obtained when the homogeneous state equation is set to $[0,0]^T$ for all future times. Let:

$$\begin{bmatrix} \dot{x}_{d1} \\ \dot{x}_{d2} \end{bmatrix} = \begin{bmatrix} 0 & 1 \\ -\dfrac{k_{i\_d}}{L_d} & -\dfrac{k_{p\_d} + R_s}{L_d} \end{bmatrix} \begin{bmatrix} x_{d1} \\ x_{d2} \end{bmatrix} \equiv \begin{bmatrix} 0 \\ 0 \end{bmatrix} \tag{50}$$

Form equation (50), equation (51) can be obtained.

$$\begin{cases} \dot{x}_{d1} = x_{d2} \equiv 0 \\ \dot{x}_{d2} = -\dfrac{k_{i\_d}}{L_d} x_{d1} - \dfrac{k_{p\_d} + R_s}{L_d} x_{d2} \equiv 0 \end{cases} \tag{51}$$

It is obvious that $x_{d1} = 0$ and $x_{d2} = 0$. Thus, the equilibrium state of the d-loop is 0 and unique.

Lemma:

Lyapunov large scale asymptotic stability theory: x_e is the equilibrium state. If there exists a scalar function $V(x)$ in the whole state space of X where:

(i) $V(x)$ and $\dot{V}(x)$ are continuous.

(ii) $V(x)$ is positive definite.

(iii) $\dot{V}(x)$ is negative semi-definite.

(iiii) For $\forall x \in X$, $\dot{V}(x) \equiv 0$ $x = x_e$ is true.

(iiiii) $\lim_{\|x\| \to \infty} V(x) = \infty$ $x \in X$.

Then system achieves large scale asymptotic stability at the equilibrium state.

Firstly, a continuous scalar function $V_d(x_d)$ is selected as is shown in equation (52). Equation (19) is brought into equation (52). Then $V_d(x_d)$ can be expressed as is shown in equation (53).

$$V_d(x_d) = \frac{K_{i\_d}}{L_d} x_{d1}^2 + x_{d2}^2 \tag{52}$$

$$V_d(x_d) = \omega_{nd}^2 x_{d1}^2 + x_{d2}^2 > 0 \tag{53}$$

Thus, $V_d(x_d)$ is continuous and positive definite.

Secondly, the partial derivative of $V_d(x_d)$ with respect to t can be obtained. $\dot{V}_d(x_d)$ is available and continuous as is shown in equation (54).

$$\dot{V}_d(x_d) = 2\omega_{nd}^2 x_{d1} \dot{x}_{d1} + 2 x_{d2} \dot{x}_{d2} \tag{54}$$

Equations (18) and (48) are brought into equation (54). Then $\dot{V}_d(x_d)$ can be expressed as is shown in equation (55).

$$\begin{aligned} \dot{V}_d(x_d) &= \\ 2\omega_{nd}^2 x_{d1} x_{d2} &+ 2 x_{d2} \left(-\omega_{nd}^2 x_{d1} - \frac{K_{p\_d} + R_s}{L_d} x_{d2} \right) \\ &= -2 \frac{K_{p\_d} + R_s}{L_d} x_{d2}^2 \\ &= -4\omega_{nd} \left(\frac{1}{(4(\cot\gamma_d)^2 + 2)^2 - 4} \right)^{\frac{1}{4}} x_{d2}^2 \le 0 \end{aligned} \tag{55}$$

Thus, $\dot{V}_d(x_d)$ is available, continuous and negative semi-definite.

Thirdly, for $\forall x_d \in X_d$, assume that $\exists x_d \neq \boldsymbol{0}$ and $\dot{V}_d(x_d) \equiv 0$ are true.

According to equation (55), if $\dot{V}_d(x_d) \equiv 0$ is true, $x_{d2} \equiv 0$ is true.

If $x_{d2} \equiv 0$ is true, $\dot{x}_{d2} \equiv 0$ is true.

According to equations (50) and (51), if $x_{d2} \equiv 0$ and $\dot{x}_{d2} \equiv 0$ are true, $x_{d1} = 0$ is true.

It is contradictory between $x_{d1} = 0$ and $x_{d2} = 0$ and the assumption.

Thus, for $\forall x_d \in X_d$, $\dot{V}_d(x_d) \equiv 0$ $x_d = \boldsymbol{0}$ is true.

Fourthly, the condition shown in equation (56) is satisfied in equation (53).

$$\lim_{\|x\|\to\infty} V_d(x_d) = \lim_{\|x\|\to\infty} \omega_{nd}^2 x_{d1}^2 + x_{d2}^2 = \infty \quad x_d \in X_d \quad (56)$$

Based on the Lyapunov large scale asymptotic stability theory, the d-loop achieves large scale asymptotic stability at the equilibrium state.

According to an analysis of the stability of the d-loop, the state vector x_q for the q-loop is defined as is shown in equation (57), and X_q is the state space of the q-loop.

$$x_q = [x_{q1}, x_{q2}]^T \in X_q \quad (57)$$

The state equation of the q-loop, the homogeneous state equation of the q-loop and the output equation of the q-loop can be obtained as is shown in equations (58), (59) and (60), respectively.

$$\begin{bmatrix} \dot{x}_{q1} \\ \dot{x}_{q2} \end{bmatrix} = \begin{bmatrix} 0 & 1 \\ -\dfrac{k_{i\_q}}{L_q} & -\dfrac{k_{p\_q}+R_s}{L_q} \end{bmatrix} \begin{bmatrix} x_{q1} \\ x_{q2} \end{bmatrix} + \begin{bmatrix} 0 \\ 1 \end{bmatrix} r_q \quad (58)$$

$$\begin{bmatrix} \dot{x}_{q1} \\ \dot{x}_{q2} \end{bmatrix} = \begin{bmatrix} 0 & 1 \\ -\dfrac{k_{i\_q}}{L_q} & -\dfrac{k_{p\_q}+R_s}{L_q} \end{bmatrix} \begin{bmatrix} x_{q1} \\ x_{q2} \end{bmatrix} \quad (59)$$

$$y_q = \begin{bmatrix} \dfrac{k_{i\_q}}{L_q} & \dfrac{k_{p\_q}}{L_q} \end{bmatrix} \begin{bmatrix} x_{q1} \\ x_{q2} \end{bmatrix} \quad (60)$$

The equilibrium state of the q-loop is $\boldsymbol{0}$ and unique.

$V_q(x_q)$ is selected for the q-loop as is shown in equation (61). Equation (21) is brought into equation (61). Then $V_q(x_q)$ can be expressed as is shown in equation (62).

$$V_q(x_q) = \frac{K_{i\_q}}{L_q} x_{q1}^2 + x_{q2}^2 \quad (61)$$

$$V_q(x_q) = \omega_{nq}^2 x_{q1}^2 + x_{q2}^2 > 0 \quad (62)$$

Thus, $V_q(x_q)$ is continuous and positive definite.

The partial derivative of $V_q(x_q)$ with respect to t can be obtained. $\dot{V}_q(x_q)$ can be expressed as is shown in equation

(63). $\dot{V}_q(x_q)$ is available, continuous and negative semi-definite.

$$\dot{V}_q(x_q) = 2\omega_{nq}^2 x_{q1} \dot{x}_{q1} + 2x_{q2} \dot{x}_{q2}$$

$$= 2\omega_{nq}^2 x_{q1} x_{q2} + 2x_{q2}\left(-\omega_{nq}^2 x_{q1} - \frac{K_{p\_q}+R_s}{L_q} x_{q2}\right)$$

$$= -2\frac{K_{p\_q}+R_s}{L_q} x_{q2}^2 \quad (63)$$

$$= -4\omega_{nq}\left(\frac{1}{(4(\cot\gamma_q)^2+2)^2-4}\right)^{\frac{1}{4}} x_{q2}^2 \leq 0$$

For $\forall x_q \in X_q$, $\dot{V}_q(x_q) \equiv 0$ $x_q = \boldsymbol{0}$ is true.

$$\lim_{\|x\|\to\infty} V_q(x_q) = \lim_{\|x\|\to\infty} \omega_{nq}^2 x_{q1}^2 + x_{q2}^2 = \infty \quad x_q \in X_q \text{ is true.}$$

Based on the Lyapunov large scale asymptotic stability theory, the q-loop achieves large scale asymptotic stability at the equilibrium state.

V. EXPERIMENTAL RESULTS

A. Experiment Platform

A 30kW PMSM is adopted for a number of experiments, and some of the parameters are shown in Table I. The effectiveness of the proposed method is verified on the experimental bench of the PMSM drive system, as is shown in Fig. 3.

B. Parameter Estimation of L_d and L_q

The estimation values of L_d and L_q of the PMSM are shown in Fig. 4.

With an increase of estimation times, the mean and variance values of L_d and L_q are calculated, as is shown in Fig. 5.

From Fig. 4 and Fig. 5, it can be seen that the estimation value of L_q is about 0.9414mH and that the estimation value of L_d is about 0.3163mH. Furthermore, even with an increase of the estimation times, the mean values of the estimation values of L_d and L_q tend to converge, and the variance values of the estimation values of L_d and L_q are about 0 and also tend to converge. Therefore, it is easy to make a judgment that the estimation values are equal to the real value.
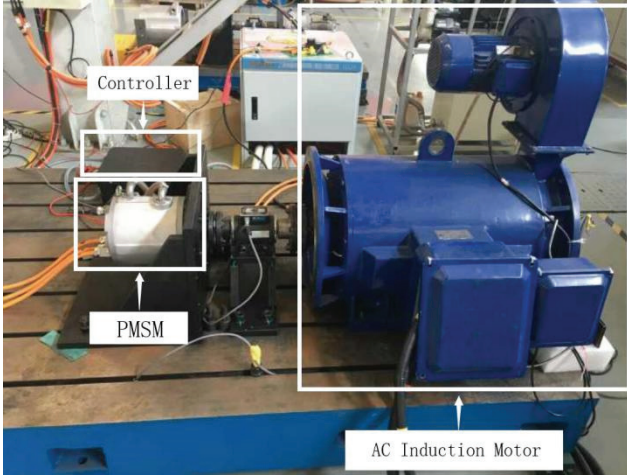
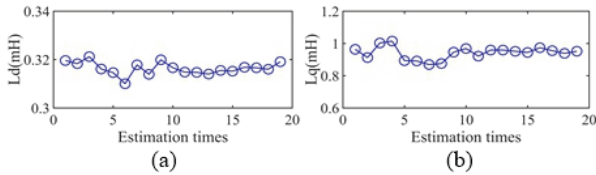Fig. 3. Experimental bench of the PMSM drive system.

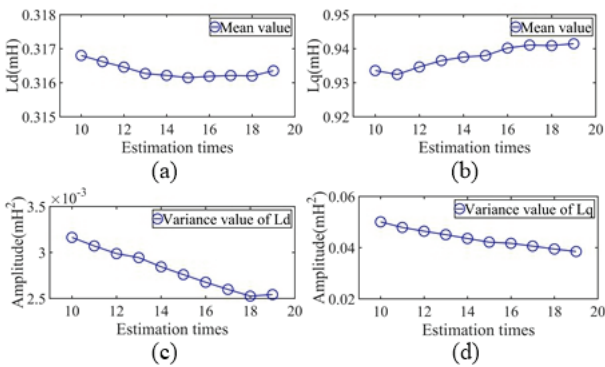Fig. 4. Estimation values of L_d and L_q. (a) Estimation values of L_d. (b) Estimation values of L_q.

Fig. 5. Mean and variance values of L_d and L_q. (a) Mean value of L_d. (b) Mean value of L_q. (c) Variance value of L_d. (d) Variance value of L_q.

C. Parameter Design of PI Controller

In this paper, according to the results of the Lyapunov stability analysis, the effects of the phase margin on the stability and response speed and the results of the modal analysis, the natural angular frequency of the *d*-loop is selected as ω_{nd}=254rad/s; the phase margin of the *d*-loop is selected as γ_d=1.51rad; the natural angular frequency of the *q*-loop is selected as ω_{nq}=423rad/s; and the phase margin of the *q*-loop is selected as γ_q=1.55rad. Then according to equations (35) through (38), the design results of the PI controller parameters are: K_{p_d}=0.9085, K_{i_d}=56.4835, K_{p_q}=0.9248, and K_{i_q}=56.5416. Thus, the experiments on different work conditions are finished.
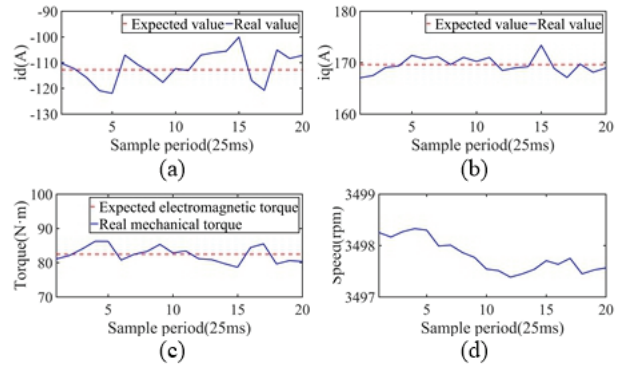
In condition 1, the PMSM is operated in the rated speed

Fig. 6. Results in condition 1. (a) i_d. (b) i_q. (c) Torque. (d) Speed.
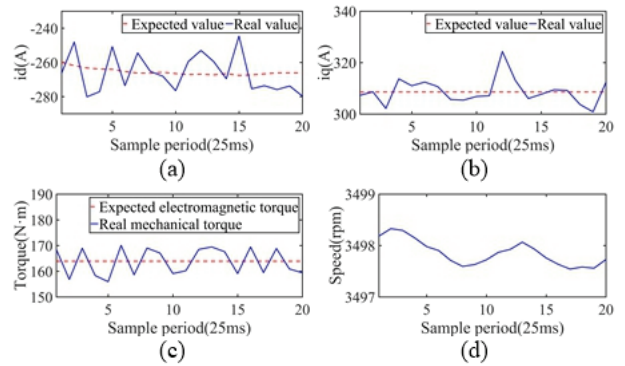

Fig. 7. Results in condition 2. (a) i_d. (b) i_q. (c) Torque. (d) Speed.

and rated power condition. That is to say, the rated speed is 3500rpm and the rated power is 30kW. The results of this condition are shown in Fig. 6. It can be seen that the fluctuation range of the real i_d is ±12.7A; the fluctuation range of the real i_q is ±3.8A; the fluctuation range of the torque is ±3.8N·m; and the fluctuation range of the speed is ±2.6rpm. Thus, the fluctuations are small in the real i_d, real i_q, torque and speed. That is to say, there is good static performance in condition 1.

In condition 2, the PMSM is operated in the rated speed and maximum power condition. That is to say, the rated speed is 3500rpm; and maximum power is 60kW. The results of this condition are shown in Fig. 7. It can be seen that the fluctuation range of the real i_d is ±23A; the fluctuation range of the real i_q is ±15.8A; the fluctuation range of the torque is ±8N·m; and the fluctuation range of the speed is ±2.5rpm. Thus, the fluctuations are small in the real i_d, real i_q, torque and speed. That is to say, there is good static performance in condition 2.

In condition 3, the PMSM is operated in the maximum speed and rated power condition. That is to say, the maximum speed is 8000rpm; and the rated power is 30kW. The results of this condition are shown in Fig. 8. It can be seen that the fluctuation range of the real i_d is ±27.83A; the fluctuation range of the real i_q is ±18.65A; the fluctuation range of the torque is ±4.2N·m; and the fluctuation range of the speed is ±4.4rpm. Thus, the fluctuations are small in the real i_d, real i_q,

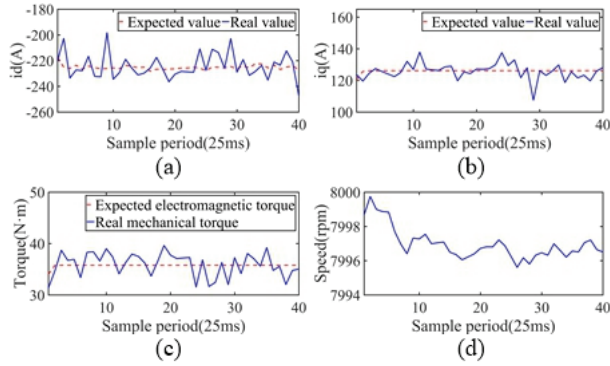Fig. 8. Results in condition 3. (a) i_d. (b) i_q. (c) Torque. (d) Speed.

Fig. 10. Results in condition 5. (a) i_d. (b) i_q. (c) Torque. (d) Speed.

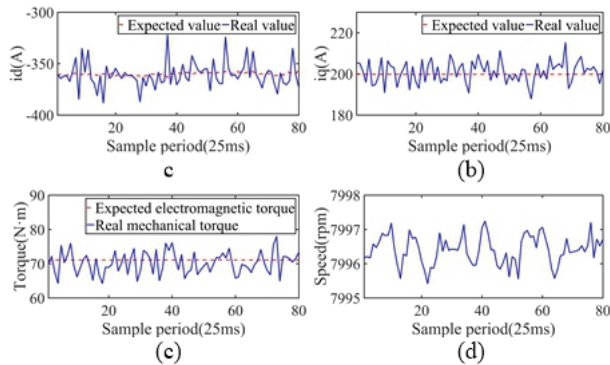Fig. 9. Results in condition 4. (a) i_d. (b) i_q. (c) Torque. (d) Speed.
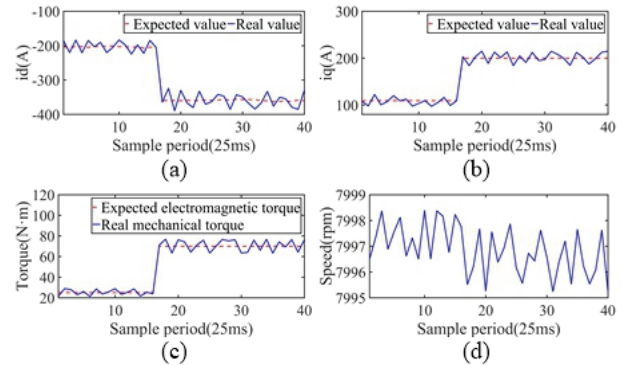
Fig. 11. Results in condition 6. (a) i_d. (b) i_q. (c) Torque. (d) Speed.

torque and speed. That is to say, there is good static performance in condition 3.

In condition 4, the PMSM is operated in the maximum speed and maximum power condition. That is to say, the maximum speed is 8000rpm; and the maximum power is 60kW. The results of this condition are shown in Fig. 9. It can be seen that the fluctuation range of the real i_d is ±36.5A; the fluctuation range of the real i_q is ±15.4A; the fluctuation range of the torque is ±6.9N·m; and the fluctuation range of the speed is ±5rpm. Thus, the fluctuations are small in the real i_d, real i_q, torque and speed. That is to say, there is a good static performance in condition 4.

In condition 5, the PMSM is operated with a sudden load when the speed is 3500rpm. At the 16th sample period, the expected electromagnetic torque is suddenly changed from 72N·m to 163N·m. The results of this condition are shown in Fig. 10. When the sample period is between the 1st and the 16st, it can be seen that the fluctuation range of the real i_d is ±8.4A; the fluctuation range of the real i_q is ±3.1A; the fluctuation range of the torque is ±3.4N·m; and the fluctuation range of the speed is ±2.3rpm. When the sample period is between the 17st and the 40st, it can be seen that the fluctuation range of the real i_d is ±23A; the fluctuation range of the real i_q is ±15.3A; the fluctuation range of the torque is ±6.9N·m; and the fluctuation range of the speed is ±2.6rpm. Thus, if the load is constant, the fluctuations are small in the real i_d, real i_q, torque and speed. That is to say, there is a good
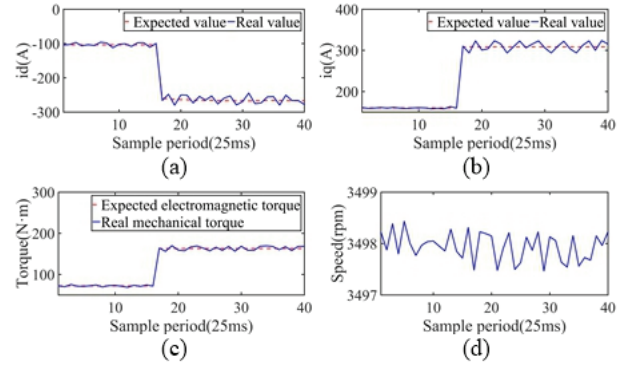
static performance in condition 5. Furthermore, if the load is changed suddenly, the real i_d, real i_q and mechanical torque can rapidly keep up with their respective expected values. Thus, there is good dynamic performance in condition 5.

In condition 6, the PMSM is operated with a sudden load when the speed is 8000rpm. At the 16th sample period, the expected electromagnetic torque is suddenly changed from 25N·m to 70N·m. The results of this condition are shown in Fig. 11. When the sample period is between the 1st and the 16st, it can be seen that the fluctuation range of the real i_d is ±19.9A; the fluctuation range of the real i_q is ±13.1A; the fluctuation range of the torque is ±3.9N·m; and the fluctuation range of the speed is ±4.4rpm. When the sample period is between the 17st and the 40st, it can be seen that the fluctuation range of the real i_d is ±35.7A; the fluctuation range of the real i_q is ±15.1A; the fluctuation range of the torque is ±6.9N·m; and the fluctuation range of the speed is ±4.8rpm. Thus, if the load is constant, the fluctuations are small in the real i_d, real i_q, torque and speed. That is to say, there is good static performance in condition 6. Furthermore, if load is changed suddenly, the real i_d, real i_q and mechanical torque can rapidly keep up with their respective expected values. Thus, there is good dynamic performance in condition 6.

In conclusion, the estimation values show that there is good accuracy in the parameter estimation method proposed in this paper. Meanwhile, if the load is constant, the fluctuations are small in the real i_d, real i_q, torque and speed. That is to say,

there is good static performance in the designed PI controller proposed in this paper. Furthermore, if load is suddenly changed, the real i_d, real i_q and mechanical torque can rapidly keep up with their respective expected values. Thus, there is good dynamic performance in the designed PI controller proposed in this paper.

VI. CONCLUSIONS

In order to design a PI controller with good performance when motor parameters are unknown, a control algorithm based on the stability margin is proposed in this paper. First of all, based on the mathematical model of the PMSM and the LS method, the motor parameters are estimated offline. Then based on the estimated values of the motor parameters, natural angular frequency and phase margin, a PI controller is designed. Performance indices including the natural angular frequency and phase margin are directly used to design the PI controller in this paper. Scalar functions of the d-loop and the q-loop are selected. It can be seen that the designed controller parameters satisfy Lyapunov large scale asymptotic stability theory if the natural angular frequencies of the d-loop and the q-loop are large than 0. Experimental results show that there is good accuracy in the parameter estimation method and that there are good static and dynamic performances in the designed PI controller. The parameter estimation method proposed in this paper is simple and easy to implement. Meanwhile, performance indices are directly used to design the PI controller and the PI controller design method is easy to implement. The PI controller design method proposed in this paper can be applied to improve design efficiency when motor parameters are unknown.

ACKNOWLEDGMENT

REFERENCES

[1] Y. Cho, K. B. Lee, J. H. Song, and Y. I. Lee, "Torque-ripple minimization and fast dynamic scheme for torque predictive control of permanent-magnet synchronous motors," *IEEE Trans. Power Electron.*, Vol. 30, No. 4, pp. 2182-2190, Apr. 2015.

[2] Y. Zhou, H. Li, and H. Zhang, "Model-free deadbeat predictive current control of a surface-mounted permanent magnet synchronous motor drive system," *J. Power Electron.*, Vol. 18, No. 1, pp. 103-115, Jan. 2018.

[3] R. Ni, D. Xu, G. Wang, L. Ding, G. Zhang, and L. Qu, "Maximum efficiency per ampere control of permanent-magnet synchronous machines," *IEEE Trans. Ind. Electron.*, Vol. 62, No. 4, pp. 2135-2143, Apr. 2015.

[4] L. Wang, K. Xiao, L. De Lillo, L. Empringham, and P. Wheeler, "PI controller relay auto-tuning using delay and

phase margin in PMSM drives," *Chin. J. Aeronaut.*, Vol. 27, No. 6, pp. 1527-1537, Dec. 2014.

[5] B. Saidi, M. Amairi, S. Najar, and M. Aoun, "Bode shaping-based design methods of a fractional order PID controller for uncertain systems," *Nonlinear Dyn.*, Vol. 80, No. 4, pp. 1817-1838, Jun. 2015.

[6] A. S. Bazanella, L. F. A. Pereira, and A. Parraga, "A new method for PID tuning including plants without ultimate frequency," *IEEE Trans. Control Syst. Technol.*, Vol. 25, No. 2, pp. 637-644, Mar. 2017.

[7] F. Haugen and B. Lie, "Relaxed Ziegler-Nichols closed loop tuning of PI controllers," *Modeling Identification and Control*, Vol. 34, No. 2, pp. 83-97, Feb. 2013.

[8] D. Valerio and J. S. Da Costa, "Tuning of fractional PID controllers with Ziegler–Nichols-type rules," *Signal Process.*, Vol. 86, No. 10, pp. 2771-2784, Oct. 2006.

[9] N. Merayo, D. Juárez, J. C. Aguado, I. De Miguel, R. J. Durán, P. Fernández, R. Mateo Lorenzo, and E. J. Abril, "PID controller based on a self-adaptive neural network to ensure QoS bandwidth requirements in passive optical networks," *J. Opt. Commun. Networking*, Vol. 9, No. 5, pp. 433-445, May 2017.

[10] J. Yu, P. Shi, W. Dong, B. Chen, and C. Lin, "Neural network-based adaptive dynamic surface control for permanent magnet synchronous motors," *IEEE Trans. Neural Networks Learn. Syst.*, Vol. 26, No. 3, pp. 640-645, Mar. 2014.

[11] M. H. Chebre, A. Meroufel, and Y. Bendaha, "Speed control of induction motor using genetic algorithm-based PI controller," *Acta Polytechnica Hungarica*, Vol. 8, No. 6, pp. 141-153, 2011.

[12] J. W. Perng, S. C. Hsieh, L. S. Ma, and G. Y. Chen, "Design of robust PI control systems based on sensitivity analysis and genetic algorithms," *Neural Comput. Appl.*, Vol. 29, No. 4, pp. 913-923, Jul. 2016.

[13] S. Li and H. Gu, "Fuzzy adaptive internal model control schemes for PMSM speed-regulation system," *IEEE Trans. Ind. Informat*, Vol. 8, No. 4, pp. 767-779, Jun. 2012.

[14] K. Devi, S. Gautam, and D. Nagaria, "Speed control of 3-phase induction motor using self-tuning fuzzy PID controller and conventional PID controller," *Int. J. Inform. Commun. Technol.*, Vol. 4, No. 12, pp. 1185-1193, 2014.

[15] A. S. Oshaba, E. S. Ali, and S. M. Abd Elazim, "PI controller design using artificial bee colony algorithm for MPPT of photovoltaic system supplied DC motor-pump load," *Complexity*, Vol. 21, No. 6, pp. 99-111, Mar. 2016.

[16] G. Durgasukumar, T. R. S. Redddy, and B. Pakkiraiah, "PID controller tuning using co-efficient diagram method for indirect vector controlled drive," *J. Electr. Eng. Technol.*, Vol. 12, No. 5, pp. 1821-1834, Sep. 2017.

[17] J. Xi, Z. Dong, Y. Ding, P. Liu, and H. Ding, "An adaptive 2DoF P-PI controller based on an improved just-in-time learning technique for ultra-low-velocity linear stages driven by PMLSMs," *Precision Eng.*, Vol. 52, pp. 392-406, Apr. 2018.

[18] S. Zheng, X. Tang, B. Song, S. Lu, and B. Ye, "Stable adaptive PI control for permanent magnet synchronous motor drive based on improved JITL technique," *ISA Trans.*, Vol. 52, No. 4, pp. 539-549, Jul. 2013.

[19] S. M. Gadoue, D. Giaouris, and J. W. Finch, "MRAS

sensorless vector control of an induction motor using new sliding-mode and fuzzy-logic adaptation mechanisms," *IEEE Trans. Energy Convers.*, Vol. 25, No. 2, pp. 394-402, Jun. 2010.

[20] C. Zhong and Y. Lin, "Model reference adaptive control (MRAC)-based parameter identification applied to surface-mounted permanent magnet synchronous motor," *Int. J. Electron.*, Vol. 104, No. 11, pp. 1854-1873, Apr. 2017.

[21] T. Boileau, N. Leboeuf, B. Nahid-Mobarakeh, and F. Meibody-Tabar, "Online identification of PMSM parameters: Parameter identifiability and estimator comparative study," *IEEE Trans. Ind. Appl.*, Vol. 47, No. 4, pp. 1944-1957, Jul. 2011.

[22] Y. Shi, K. Sun, L. Huang, and Y. Li, "Online identification of permanent magnet flux based on extended Kalman filter for IPMSM drive with position sensorless control," *IEEE Trans. Ind. Electron.*, Vol. 59, No. 11, pp. 4169-4178, Nov. 2012.

[23] K. Liu, Q. Zhang, J. Chen, Z. Q. Zhu, and J. Zhang, "Online multiparameter estimation of nonsalient-pole PM synchronous machines with temperature variation tracking," *IEEE Trans. Ind. Electron.*, Vol. 58, No. 5, pp. 1776-1788, May 2011.

[24] K. Liu , Z. Q. Zhu, and D. A. Stone, "Parameter estimation for condition monitoring of PMSM stator winding and rotor permanent magnets," *IEEE Trans. Ind. Electron.*, Vol. 60, No. 12, pp. 5902-5913, Dec. 2013.

[25] K. H. Kim, S. K. Chung, G. W. Moon, I. C. Baik, and M. J. Youn, "Parameter estimation and control for permanent magnet synchronous motor drive using model reference adaptive technique," in *Proc. IECON*, pp. 387-392, 1995.

[26] Z. H. Liu, J. Zhang, X. H. Li, and Y. J. Zhang, "Immune co-evolution particle swarm optimization for permanent magnet synchronous motor parameter identification," *Acta Autom. Sin.*, Vol. 38, No. 10, pp. 1698-1708, 2012.

[27] K. Wang, J. Chiasson, M. Bodson, and L. M. Tolbert, "A nonlinear least-squares approach for identification of the induction motor parameters," *IEEE Trans. Autom. Contr.*, Vol. 50, No. 10, pp. 1622-1628, Oct. 2005.

[28] Y. Wang, S. Xu, H. Huang, Y. Guo, and H. Jin, "A coupled recursive total least squares-based online parameter estimation for PMSM," *J. Electr. Eng. Technol.*, Vol. 13, No. 6, pp. 2344-2353, Nov. 2018.

[29] Z. Shi, Y. Wang, and Z. Ji, "Bias compensation based partially coupled recursive least squares identification algorithm with forgetting factors for MIMO systems: Application to PMSMs," *J. Franklin Inst.*, Vol. 353, No. 13, pp. 3057-3077, Sep. 2016.

Hongyu Jie was born in Inner Mongolia, China, in 1992. He received his B.S. degree in Automation from the University of Electronic Science and Technology of China, Chengdu, China, in 2014, where he has been working towards his Ph.D. degree since 2016. His current research interests include motor driver technology, electric vehicle control and electric ship propulsion systems.

Hongbing Xu received his M.S. degree in Automatic Control from Southeast University, Nanjing, China, in 1988; and his Ph.D. degree in Automation from the University of Electronic Science and Technology of China, Chengdu, China, in 2000. He is presently working as a Professor at the University of Electronic Science and Technology of China. His current research interests include motor driver technology, active safety systems for electric vehicles and electric ship propulsion systems.

Yanbing Zheng received his B.S. degree in Automation from the University of Electronic Science and Technology of China, Chengdu, China, in 2016, where he is presently working towards his M.S. degree. His current research interests include new energy and current control for distributed systems.

Xiaoshuai Xin received his B.S., M.S. and Ph.D. degrees in Automation from the University of Electronic Science and Technology of China, Chengdu, China, in 2006, 2009 and 2014, respectively. His current research interests include robust control and optimal control for electric vehicles.

Gang Zheng received his B.S., M.S. and Ph.D. degrees in Automation from the University of Electronic Science and Technology of China, Chengdu, China, in 2002, 2006 and 2011, respectively. His current research interests include wind power generation, power electronics, multilevel inverters, storage converters and electric ship propulsion systems.